Check for updates

**Photovoltaics** 

# Understanding of the Relationship between the Properties of Cu(In,Ga)Se<sub>2</sub> Solar Cells and the Structure of Ag Network Electrodes

Hyesun Yoo , Hoang Van Quy, Inpyo Lee, Seung Taek Jo, Tae Ei Hong, JunHo Kim, Dae-Hwang Yoo, Jinwook Shin, Walter Commerell, Dae-Hwan Kim\*, and Jong Wook Roh\*

The relation between the structure of the silver network electrodes and the properties of Cu(In,Ga)Se2 (CIGS) solar cells is systemically investigated. The Ag network electrode is deposited onto an Al:ZnO (AZO) thin film, employing a self-forming cracked template. Precise control over the cracked template's structure is achieved through careful adjustment of temperature and humidity. The Ag network electrodes with different coverage areas and network densities are systemically applied to the CIGS solar cells. It is revealed that predominant fill factor (FF) is influenced by the figure of merit of transparent conducting electrodes, rather than sheet resistance, particularly when the coverage area falls within the range of 1.3-5%. Furthermore, a higher network density corresponds to an enhanced FF when the coverage areas of the Ag networks are similar. When utilizing a thinner AZO film, CIGS solar cells with a surface area of 1.0609 cm<sup>2</sup> exhibit a notable performance improvement, with efficiency increasing from 10.48% to 11.63%. This enhancement is primarily attributed to the increase in FF from 45% to 65%. These findings underscore the considerable potential for reducing the thickness of the transparent conductive oxide (TCO) in CIGS modules with implications for practical applications in photovoltaic technology.

Dr. H. Yoo, I. Lee, S. T. Jo, Dr. D.-H. Yoo, J. Shin, Prof. J. W. Roh Regional Leading Research Center (RLRC) of Smart Energy System, Kyungpook National University, Gyeongsangbuk-do 37224, Korea E-mail: jw.roh@knu.ac.kr

Dr. H. Van Quy, Dr. D.-H. Kim

Division of Energy Technology, Daegu—Gyeongbuk Institute of Science and Technology (DGIST), Daegu 42988, Korea

E-mail: monolith@dgist.ac.kr

I. Lee, S. T. Jo, J. Shin, Prof. J. W. Roh

Department of Hydrogen and Renewable Energy, Kyungpook National University, Daegu 47922, Korea

T. E. Hong, Prof. J. Kim

Nano Photoelectronic Device Lab, Department of Physics, Incheon National University, Incheon 22012, Korea

Prof. W. Commerell

Institute for Energy and Drive Technology, Technische Hochschule Ulm (THU), Ulm 89081, Germany

Prof. J. W. Roh

Department of Nano & Advanced Materials Science and Engineering, Kyungpook National University, Gyeongsangbuk-do 37224, Korea

The ORCID identification number(s) for the author(s) of this article can be found under https://doi.org/10.1002/eem2.12765.

DOI: 10.1002/eem2.12765

#### 1. Introduction

In the field of solar energy, the promise of thin film technologies embodied by Cu(In,Ga)Se2 (CIGS) and perovskite solar cells lies in their remarkable ability to reduce module thickness. This attribute not only results in lightweight configurations but also enables the creation of flexible solar modules. These inherent benefits have positioned thin-film solar cells as promising contenders for the next generation of solar technology, potentially replacing traditional Si solar cells. The fabrication process of thin-film solar modules typically involves the monolithic integration of subcells, a technique faced with two major challenges: resistive losses in transparent conductive oxides (TCO) and the occurrence of dead areas.[1-4] The resistive losses are particularly problematic as the conductivity of TCO decreases with increased length, which restricts the width of individual subcells to about 4–5 mm to reduce these losses.<sup>[4,5]</sup> Additionally, this limitation necessitates more frequent P1P2P3 scribing, leading to increased

dead areas and degradation of the thin film, [1,4-6] which significantly contributes to the efficiency gap between solar modules and laboratory-scale cells.

Addressing these challenges, the application of a metal grid to the TCO as a front contact has been explored as an effective method to improve solar module performance by increasing the monolithic width. [1,3,5–7] Research into the optimal structure of the metal grid has indicated that finger widths of 20–40  $\mu m$  enhance the efficiency of solar cells. [3–7] However, the relatively large width of the metal grid presents integration challenges in building structures and semi-transparent solar cells, particularly in terms of architectural design and aesthetics. [8] Moreover, the reliance on expensive patterning techniques for strip lines, such as conventional lithography, has prompted investigations into simpler, cost-effective methods for applying metallic transparent electrodes. [8–16]

The utilization of a self-formable cracked template represents a more straightforward and accessible approach compared with conventional lithography for manufacturing purposes. This method involves applying a solution to a substrate via spin coating, followed by a natural drying process that induces crack formation, serving as sacrificial templates. [11,12,17–19] Such a technique facilitates the production of

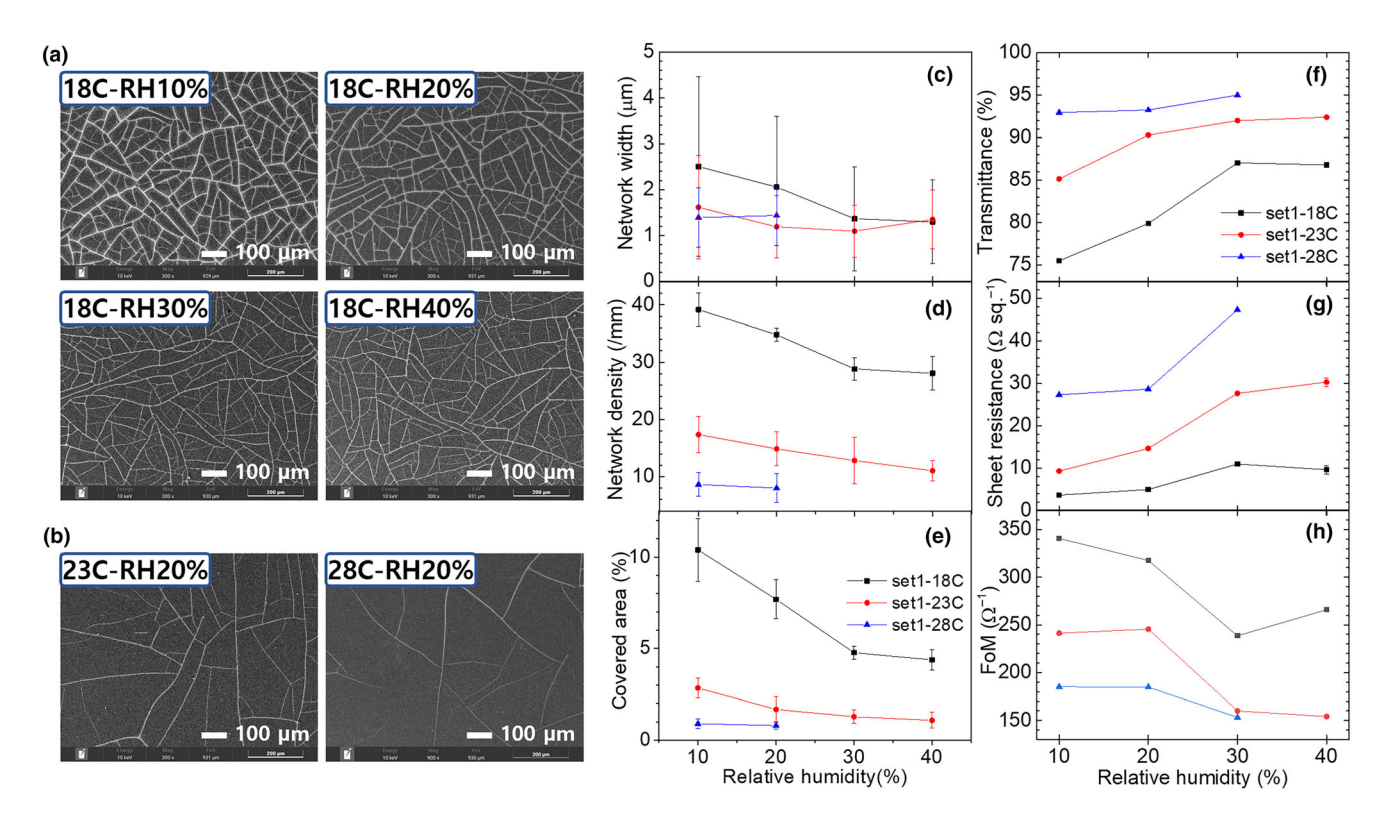


**Figure 1.** SEM images of Ag networks in Set1 series a) fabricated at  $\sim$ 18 °C under varying humidity levels from 10% RH to 40% RH, and b) fabricated at different temperatures under 20% RH. The Ag network characteristics include c) width, d) density, and e) CA, while their optical and electrical properties encompass f) transmittance, g) sheet resistance, and h) the figure of merit for TCE. Notably, Set1-28C-RH30 and -RH40 samples lack structural information in (c–e) due to the absence of cracks in the sample.

metallic networks with a wide range of line widths, varying from less than 1  $\mu$ m to tens of micrometers. The adaptability of this method has catalyzed extensive research in various applications, including light-emitting diodes, [16,20] transparent heaters, [18,21,22] sensors, [22,23] smart windows, [17,24] and solar cells. [11,12,15,17,19,25] The current study employs this technique to explore the relationship between the structures of silver networks and the properties of CIGS solar cells, aiming to optimize the Ag network electrode to improve solar cell efficiency. Additionally, this research investigates the potential for reducing the thickness of the TCO in CIGS solar cells through the application of an Ag network.

#### 2. Results and Discussion

#### 2.1. Controlling the Structures of Ag Mesh-like Network

The structure of the self-forming cracked template for the Ag network was effectively controlled by manipulating the humidity and temperature during the drying conditions. Figure S1, Supporting Information, presents images of the hybrid transparent conducting electrodes (TCEs), demonstrating their transparency. Scanning electron microscopy (SEM) images of the Ag networks depicted in **Figure 1a**,b clearly demonstrate that both network widths and densities increase as the temperature and humidity decrease, ranging from 40% RH to 10% RH and from ~28 to 18 °C, respectively. For instance, the SEM image of the sample fabricated at 18 °C under 20% RH (set1-18C-RH20) is

detailed in Figure 1a. Observations reveal an increasing trend in the covered areas of the Ag networks at all temperatures as humidity decreases. This trend indicates that the impact of network density on the covered area is more significant than that of network width. Figure 1c–e illustrate the variations in width, density, and covered area of the Ag network structure in relation to temperature and humidity. The data indicate that while the average width shows minimal variation,  $\sim 1-2.5 \, \mu m$ , the average density exhibits a broader range, from 8 to 39/mm, displaying trends similar to those observed for the covered area, as shown in Figure 1d,e. Consequently, it is clear that the covered area is predominantly determined by the network density.

As the covered area (CA) of the Ag network increases, the figure of merit (FOM) for the TCE generally rises, predominantly due to a more pronounced decrease in sheet resistance (R<sub>sh</sub>) compared with a smaller reduction in transmittance. Figure 1f—h delineate the characteristics of the hybrid TCE based on the Ag network structure. In this analysis, as humidity decreases from 40% RH to 10% RH, the transmittance marginally diminishes from 95% (for Al:ZnO (AZO) alone) to 75.5% (for the hybrid TCE), while R<sub>sh</sub> significantly drops from 47.3  $\Omega$  sq $^{-1}$  (for AZO) to 3.7  $\Omega$  sq $^{-1}$  (for the hybrid TCE). Consequently, the FOM escalates from 153 to 341/ $\Omega$ .

While  $R_{sh}$  is commonly correlated directly with the CA, the observed trends in increasing CA and decreasing  $R_{sh}$  are not exactly inversely proportional. For instance, in the set1-18C series, the CA notably rises from  $4.4 \pm 0.6\%$  to  $10.4 \pm 1.7\%$ , yet  $R_{sh}$  only slightly declines from 9.7 to  $3.7~\Omega$  sq<sup>-1</sup>. In contrast, for the set1-23C series, the CA modestly increases from  $1.1 \pm 0.4\%$  to  $2.8 \pm 0.5\%$ , alongside a substantial

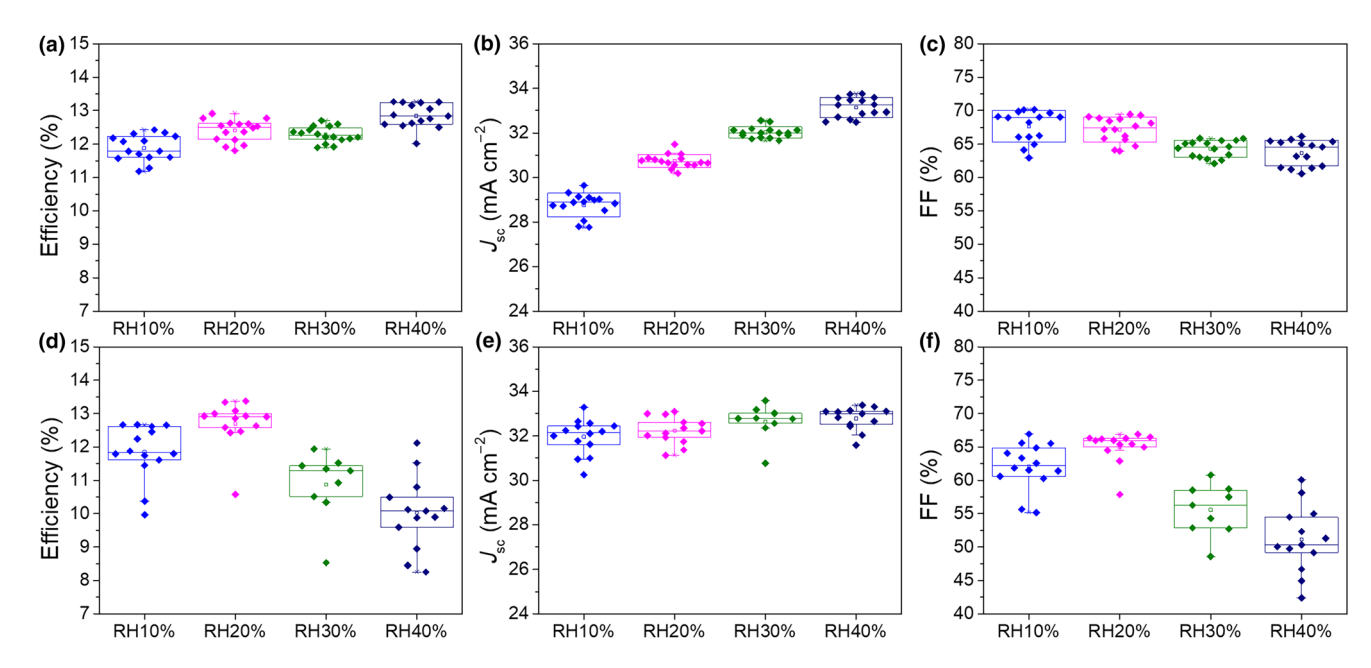


**Figure 2.** Solar cell performance, including a, d) efficiency (Eff), b, e) short-circuit current density ( $J_{sc}$ ), and c, f) fill factor (FF), for Set1-18C and Set1-23C series. The  $V_{oc}$  (open-circuit voltage) values for each series, along with the solar cell properties for Set1-28C series, are detailed in Figure S4, Supporting Information.

reduction in  $R_{sh}$  from 30.3 to 9.3  $\Omega$  sq<sup>-1</sup>. As a result, FOM enhances from 266/ $\Omega$  (at 40% RH) to 341/ $\Omega$  (at 10% RH) for set1-18C samples, and from 154/ $\Omega$  (at 40% RH) to 241/ $\Omega$  (at 10% RH) for set1-23C samples. However, deviations in this trend are observed in set1-18C-RH30 and set1-23C-RH20, which exhibit FOM values of 239 and 246/ $\Omega$ , respectively. These anomalies stem from varying trends in the decrease of  $R_{sh}$  with an increase in CA, contrasting with the trend in transmittance decrease, which shows an inverse correlation with the increase in CA.

Based on these findings, the FOM values depicted in Figure 1h can be categorized into three distinct ranges according to the CA: i) FOM greater than  $320/\Omega$  for a CA >5%, ii) FOM ranging between 190 and  $320/\Omega$  for a CA between 1.3% and 5%, and iii) FOM below  $190/\Omega$  for a CA <1.3%. This categorization indicates that the CA of the Ag network significantly influences the FOM of the TCE. The subsequent section elaborates on the correlation between the trend and value of the FOM and the average FF values for the solar cells.

### 2.2. Solar Cell Properties Depending on the Structures of Ag Networks

The attainment of the highest FOM for a TCE does not necessarily ensure the highest efficiency in the corresponding CIGS solar cells. For example, the set1-18C-RH10 sample, which demonstrates the highest FOM value of  $341/\Omega$  and a CA of  $10.4\pm1.7\%$  as shown in Figure 1h, e, paradoxically registers the lowest average efficiency (11.8%) within the set1-18C-series, as illustrated in Figure 2a. In contrast, the set1-18C-RH40 sample, with a FOM of  $266/\Omega$  and a CA of  $4.4\pm0.6\%$ , achieves the highest efficiency of 12.8% among its counterparts. The superior efficiency of the set1-18C-RH40 sample is attributed to the significant decrease in  $J_{\rm sc}$  and marginal increase in FF as humidity reduces from 40% RH to 10% RH, as depicted in Figure 2b,

c. These figures collectively display the solar cell properties of the set1-18C series in relation to humidity, distinctly revealing a sharp decline in  $J_{\rm sc}$  and a gradual ascent in FF with decreasing humidity. Since solar cell efficiency is directly proportional to both  $J_{\rm sc}$  and FF, the set1-18C-RH40 sample's performance surpasses that of its counterparts, highlighting that specific FOM values and/or CAs are more conducive to enhancing solar cell efficiency.

The relationship between  $J_{sc}$  and the CA is intuitively understandable, as the current generated is proportional to the incident light on the solar cell. However, the degree to which  $J_{sc}$  is influenced by the CA remains ambiguous. Observing Figure 2b,e, it is apparent that  $J_{sc}$  is significantly impacted when the CA of the Ag network exceeds 4%. This reduction in  $J_{sc}$  was more pronounced in the set1-18C series with decreasing humidity compared with the set1-23C series. Simultaneously, the disparities in the CAs for the set1-18C series were larger than those for the set1-23C series, as shown in Figure 1e. Considering the CAs of both the set1-18C and set1-23C series, it becomes evident that  $J_{sc}$  is considerably affected when values surpass  $\sim$ 4%. Below this threshold, the impact on  $J_{sc}$  diminishes, whereas the influence on FF becomes more pronounced.

Contrary to common expectations, the FF appears to correlate more closely with the FOM than with  $R_{\rm sh}$ , as indicated by the results. In the set1-23C series, the average FF demonstrated an upward trend as humidity decreased from 40% RH to 10% RH. Nonetheless, an exception to this pattern was noted at 20% RH for the set1-23C-RH20 sample, as illustrated in Figure 2f. If FF, which is influenced by series resistance  $(R_s)$  values, were directly associated with  $R_{\rm sh}$ , the  $R_{\rm sh}$  graph in Figure 1g would mirror the FF graph in Figure 2f. However, contrary to initial assumptions, an anomaly at 20% RH is observed in the FOM graph for the set1-23C series (represented in red) in Figure 1h. Moreover, the set1-18C-RH30 sample, displaying the lowest FOM value among the set1-18C series, unexpectedly showed an FF value akin to that of the set1-18C-RH40 sample, diverging from the general ascending trend of FF from 40% RH to 10% RH.

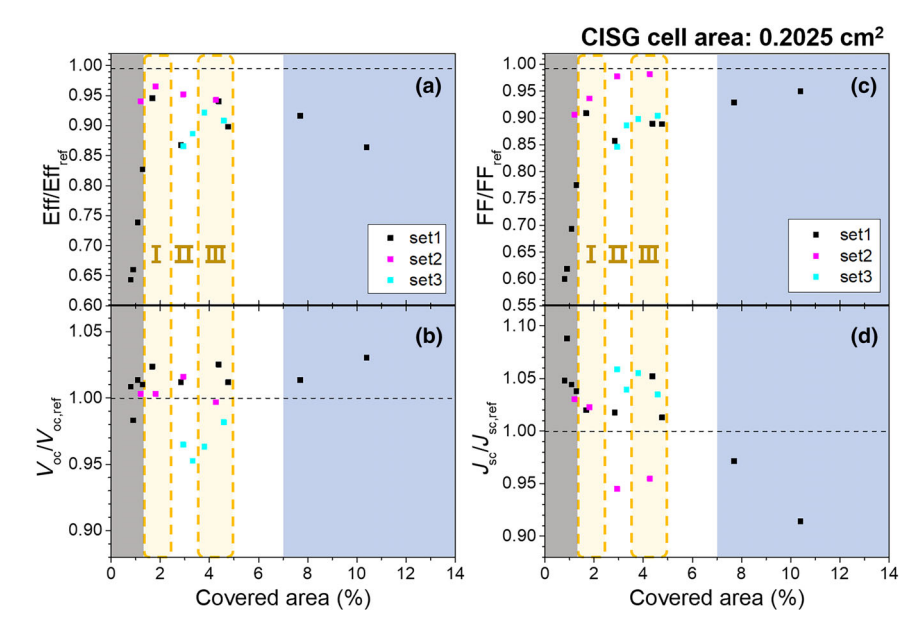


Figure 3. Relative characteristics of solar cells with a fixed area of 0.2025 cm<sup>2</sup>, dependent on the covered areas.

When the FOM value falls below  $190/\Omega$ , as seen in the set1-23C-RH30 and -RH40 samples, the decline in FF compared with the reference sample (FF<sub>ref</sub> = 72.61%, described in Table S1, Supporting Information) is more pronounced than in other samples. This trend is also evident in the set1-28C series, which has FOM values beneath  $190/\Omega$ , exhibiting a substantial discrepancy in FF between the samples and the reference (as shown in Figure S2, Supporting Information).

These observations suggest that the FOM's impact on FF is more significant than that of  $R_{\rm sh}$ . Given that the light penetrating the solar cell through the Ag network contributes to electricity generation, both transmittance and  $R_{\rm sh}$  are instrumental in actual power generation, thereby influencing the FF. Anand et al.<sup>[2]</sup> proposed a novel FOM to better estimate photovoltaic (PV) performance. Subsequently, Muzzillo updated the novel FOM formula, considering the influence of TCE on the current density and voltage at its maximum power point. Particularly, the updated FOM for PV application, as described in equation (12) of the literature, [26] correlates with the efficiency trend of CIGS solar cells. Furthermore, considering the previously discussed relationships between FOM and the CA (as in Section 2.1), it is also inferred that the deterioration of FF becomes more pronounced when the CA is <1.3%.

In **Figure 3**, the relative properties of the CIGS solar cells are depicted in relation to the reference cell, with a focus on the CAs of the

Ag networks. To encompass a broader range of CA values, set2 and set3 samples were fabricated by maintaining constant temperature and humidity while varying the spin-coating speed between 2000 and 8000 rpm. It is noteworthy that controlling the humidity and temperature conditions during the drying process (as in set1) proves more effective in achieving a diverse range of CAs for the Ag network compared with adjusting the spin-coating speed in set2 (indicated in pink) and set3 (indicated in blue). Figure 3 vividly illustrates the general trends of decreasing  $\Delta J_{sc}$  ( $J_{sc}/J_{sc}$ ref-the ratio of short-circuit current to that of the reference cell) and increasing  $\Delta FF$ (FF/FF<sub>ref</sub>—the ratio of fill factor to that of the reference cell) as the CA enlarges. Notably,  $\Delta$ FF shows a marked increase within the 0-1.3% CA range. As the CA expands, the rate of increase in  $\Delta$ FF progressively lessens. In contrast,  $\Delta J_{sc}$  attains values exceeding 103% within the 0-1.3% CA range but displays fluctuations within the 1.3-5% CA range. Beyond a 5% CA, the decreasing rate of  $\Delta J_{sc}$  becomes more pronounced.

As a result, the efficiency of CIGS solar cells can approximate that of the reference cell within a CA range of 1.3–5%. The highest values of  $\Delta Eff$  (Eff/Eff\_ef—the ratio of efficiency to that of the reference cell) for the set1, set2, and set3 series are observed at 1.7  $\pm$  0.7% CA for a 0.95, 1.8  $\pm$  0.6% CA for a 0.97, and 3.8  $\pm$  0.6% CA for a 0.92, respectively. Additionally, the second-highest  $\Delta Eff$  value for the set1 series is 0.94 at a 4.4  $\pm$  0.6% CA, as indicated in Table S1, Supporting Information. Intriguingly, the highest efficiency values were noted when the CA were around 2% (zone I) or 4% (zone III), except for  $\sim$ 3% (zone II), as demonstrated in Figure 3. The underlying cause of this phenomenon, however, remains unclear and warrants further investigation.

In some instances, notable differences in  $\Delta Eff$  values were observed among samples with similar CAs. For example, the set2 and set3 samples, fabricated at 6000 rpm (set2-6k) and 4000 rpm (set3-4k) respectively, exhibit comparable CAs of  $3.0\pm0.7\%$  and  $2.9\pm0.5\%$ , as detailed in Table 1. However, there is a disparity in their  $\Delta Eff$  values, with set2-6k showing 0.95 and set3-4k showing 0.87, attributable to differences in  $\Delta FF$ . This discrepancy is linked to variations in the density of the Ag networks. As the network density escalates from  $13.9\pm1.7/mm$  for set3-4k to  $21.2\pm2.6/mm$  for set2-6k,  $\Delta FF$  improves from 85% to 98%, respectively. A similar trend was noted between the set2-8k and set3-2k samples, indicating that within a CA range of 1.3-5%, an increase in network density can enhance FF.

Table 1. Parameters describing the Ag network structure and the relative performance of solar cells with an area of 0.2025 cm<sup>2</sup>, based on various covered areas.

Covered area	Sample name	Width [µm]	Density [per mm]	Covered area [%]	$\Delta V_{\rm oc} \; (V_{\rm oc}/V_{\rm oc,ref})$	$\Delta J_{sc} (J_{sc}/J_{sc,ref})$	$\Delta$ FF (FF/FF <sub>ref</sub> )	$\Delta \text{Eff (Eff/Eff}_{\text{ref}})$	$\Delta R_{\rm s} (R_{\rm s}/R_{\rm s,ef})$
$\sim$ 3% (Zone II)	set3-4k	$\textbf{1.9} \pm \textbf{0.45}$	$\textbf{13.9} \pm \textbf{1.7}$	$\textbf{2.9} \pm \textbf{0.5}$	0.96	1.06	0.85	0.87	3.87
	set2-6k	$\textbf{1.4} \pm \textbf{0.90}$	$\textbf{21.2} \pm \textbf{2.6}$	$\textbf{3.0} \pm \textbf{0.7}$	1.02	0.95	0.98	0.95	2.29
${\sim}4\%$ (Zone III)	set2-8k	$\textbf{1.7} \pm \textbf{1.2}$	$\textbf{26.4} \pm \textbf{2.05}$	$\textbf{4.3} \pm \textbf{0.7}$	1.00	0.95	0.98	0.94	2.35
	set3-2k	$\textbf{3.3} \pm \textbf{2.5}$	$\textbf{12.8} \pm \textbf{1.99}$	$\textbf{4.6} \pm \textbf{0.9}$	0.98	1.03	0.90	0.91	3.86

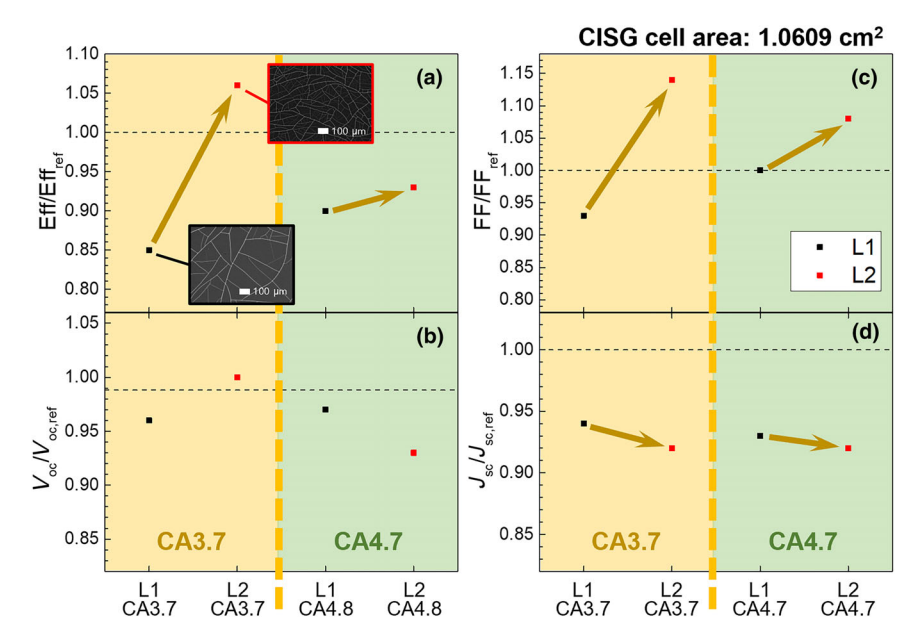


**Figure 4.** Relative performance of solar cells in L1 and L2 series a–d) and SEM images of L1-CA3.7 and L2-CA3.7 samples. Despite similar covered areas, differences in the relative performance of these solar cells arise from variations in network densities, as elucidated in the SEM images within the figure. For enlarged SEM images, please refer to Figure S3, Supporting Information.

## 2.3. Optimum Structure of Ag Network for Large-Area CISG Solar Cells

This effect of FF improvement due to elevated network density, even with similar Ag network CAs, was also discernible in larger CIGS solar cells. To investigate if similar effects could be achieved in larger cells, Ag networks were applied to a solar cell with an area of 1.0609 cm<sup>2</sup>, over five times larger than those in the set1-3 series. Figure 4 and Table 2 summarize the relative properties of four samples: two with lower density (L1) and two with higher density (L2), for covered areas of  $\sim$ 3.7% (CA3.7) and 4.7% (CA4.7). As Figure 4c and Table 2 reveal, for the L1-CA3.7 and L2-CA3.7 samples,  $\Delta$ FF markedly increases from 0.93 to 1.14 as density rises from 12.9  $\pm$  2.5/mm to 32.8  $\pm$  2.5/mm. Network densities for these samples are displayed in Figure S3c,d, Supporting Information. Despite a minor decline in  $\Delta J_{sc}$  from 0.94 to 0.92,  $\Delta$ Eff notably improves from 0.85 to 1.06, surpassing the reference cell's efficiency. The  $\Delta FF$  enhancement due to increased density is also evident in the CA4.7 samples. However, the L2-CA4.7 sample did not exceed the reference cell's efficiency, experiencing an unexplained reduction in  $\Delta V_{\rm oc}$  (the ratio of open-circuit voltage to that of the reference cell). Solar cell parameters for the L1 and L2 series, along with their respective reference cells, are shown in Figure S3a,b and Table S2, Supporting Information.

In Figure S4, Supporting Information, the J-V and external quantum efficiency (EQE) curves are displayed alongside photographs of the L2 series reference cell (L2-Ref) and L2-CA3.7 samples. The EQE curve indicates a reduction in  $J_{\rm sc}$  across wavelengths ranging from  $\sim$ 400 to 1100 nm, attributable to the coverage of the CIGS solar cell surface by the Ag network electrode. This results in a decrease in  $J_{\rm sc}$  from 34.9 to 32.1 mA cm<sup>-2</sup>, while the FF experiences an enhancement from 56.5% to 64.5%. Consequently, the L2-CA3.7 sample achieves an efficiency of 12.7%, surpassing the 12.0% efficiency of the L2-Ref. The photographs

in Figure S4c, Supporting Information, visually demonstrate the transparency of Ag networks on L2-CA3.7 compared with the L2-Ref. By employing nearly transparent Ag networks on the AZO thin film, the efficiency of the CIGS solar cell is improved without necessitating an antireflection coating or post-deposition treatment (PDT) process. These results suggest that for optimizing the efficiency of CIGS solar cells, a CA in the range of 1.3–5% with a higher density of Ag networks on the AZO thin film is recommended.

To assess the effectiveness of reducing the TCO thickness while still benefiting from the Ag network, L3 set samples were prepared with a reduced AZO film thickness, from 350 nm to 150 nm. The Ag network was then applied to these samples (L3-CA5.3) to evaluate the potential improvement in efficiency. The structure and SEM image of the Ag network utilized in the L3 series are presented in Figure S5, Supporting Information. As depicted in **Figure 5**, the CIGS solar cell with a substantially reduced AZO thickness (L3-Ref) gets the efficiency of 10.5%. In contrast, the efficiency of the L3-CA5.3 sample was enhanced to 11.6%, marking a 1.3%

improvement. Notably, the FF increased from 44.7% to 65.4%, further confirming the enhancement in efficiency. These findings validate that the application of an Ag network electrode on a thinner AZO film can significantly augment the efficiency of large-area CIGS solar cells, even when the AZO layer thickness is reduced by more than half.

#### 3. Conclusion

In conclusion, this study successfully demonstrated that the Ag mesh-like network structure was meticulously controlled by modulating temperature and humidity conditions during the drying of the coated acrylic film. This strategic approach resulted in a progressive increase in both the density and CA of the Ag networks as temperature and humidity were reduced, leading to a significant enhancement of the FOM of the TCE. The set1-18C-RH40 sample, in particular, achieved the highest FOM value of 341/ $\Omega$ , characterized by the lowest  $R_{\rm sh}$  at 3.67  $\Omega$  sq $^{-1}$  and a transmittance of 75.5% at 550 nm. However, it was observed that the attainment of the highest FOM did not necessarily correlate with the highest efficiency in the corresponding solar cell.

The efficiency of the solar cells was found to be influenced by the interplay between the increasing rate of FF and the decreasing rate of  $J_{\rm sc}$ , which varied according to the CA of the Ag networks. When the CA was within the range of 1.3–5%, the solar cells exhibited high efficiencies. In cases where the CA exceeded 5%, the rise in FF became marginal, whereas the decline in  $J_{\rm sc}$  was more pronounced, leading to a reduction in efficiency. Conversely, CAs below 1.3% resulted in minimal improvements in  $J_{\rm sc}$  but significant decreases in FF, adversely affecting efficiency. It was noteworthy that in the range of 1.3–5% CA, the FF of the solar cells was more influenced by the FOM value than by the  $R_{\rm sh}$  of the hybrid TCE. Furthermore, the study revealed that enhancing

**Table 2.** Parameters characterizing the Ag network structure and the performance of solar cells with an area of 1.0609 cm<sup>2</sup> in L1 and L2 series.

Sample name	Width [μm]	Density [per mm]	Covered area [%]	$\Delta V_{ m oc}$ $(V_{ m oc}/V_{ m oc,ref})$	$\Delta J_{sc}$ $(J_{sc}/$ $J_{sc,ref})$	ΔFF (FF/ FF <sub>ref</sub> )	ΔEff (Eff/ Eff <sub>ref</sub> )
L1-CA3.7	$\textbf{2.68} \pm \textbf{2.06}$	$\textbf{12.91} \pm \textbf{1.64}$	$\textbf{3.76} \pm \textbf{0.46}$	0.96	0.94	0.93	0.85
L2-CA3.7	$\textbf{1.07} \pm \textbf{0.92}$	$\textbf{32.76} \pm \textbf{2.48}$	$\textbf{3.69} \pm \textbf{0.13}$	1.0	0.92	1.14	1.06
L1-CA4.7	$\textbf{3.01} \pm \textbf{3.30}$	$\textbf{15.86} \pm \textbf{1.11}$	$\textbf{4.75} \pm \textbf{0.96}$	0.97	0.93	1.0	0.90
L2-CA4.7	$\textbf{1.09} \pm \textbf{1.10}$	$\textbf{40.49} \pm \textbf{4.04}$	$\textbf{4.74} \pm \textbf{0.35}$	0.93	0.92	1.08	0.93

the network density, even with similar CAs, was essential to improve the solar cell FF.

This research also extended its findings to large-area CIGS solar cells. By applying Ag networks with varying densities and CAs, it was demonstrated that the efficiency of a CIGS solar cell with an area of  $1.0609~{\rm cm}^2$  could be improved from 12.0% to 12.7% with an Ag network having a CA of 3.7 + 0.1%, a density of 32.8  $\pm$  2.5/mm, and a width of 1.1 + 0.9  $\mu m$ . Remarkably, even with a reduction in the thickness of the AZO layer by more than half (from 350 to 150 nm), the Ag network played a crucial role in enhancing the efficiency of large-area CIGS solar cells, elevating it from 10.5% to 11.6% through an improvement in FF. Additionally, this result also suggests the possibility of widening the monolithic width of the CIGS module up to 1 cm.

The findings of this study underscore the importance of carefully configuring the network structure, particularly targeting a CA of 1.3–5% and a higher network density, for the effective application of a metallic network electrode to thin-film solar cells. These insights into optimizing the Ag network, if integrated onto the TCO of the back contact of a solar cell, have the potential to be beneficial not only for traditional solar modules but also for emerging technologies such as semi-transparent and bifacial solar cells.

#### 4. Experimental Details

Fabrication of the self-formable Ag network: The electrode network of Ag was fabricated on a glass substrate coated with Al:ZnO (AZO), measuring 2.5 × 2.5 cm², and on a CIGS solar cell. This fabrication utilized acrylic resin (Carboset CR795, Lubrizol) applied through a spin-coating method, as depicted in Figure 6. The acrylic resin was diluted with DI water in a volume ratio of 85:15, as the undiluted acrylic resin failed to form cracks at room temperature. The AZO-coated glass substrate served to evaluate the characteristics of a TCE, whereas the AZO thin film applied on a CIGS solar cell was employed to study the solar cell properties influenced by different Ag network structures.

In both scenarios, the Ag network fabrication involved the following procedure: Initially,  $O_2$  plasma treatment was administered to the AZO thin film surface to enhance its hydrophilicity, a crucial factor affecting the spreading and cracking behaviors of the acrylic resin  $^{[10]}$  Subsequently, the diluted acrylic resin was dispensed onto the hydrophilic-treated AZO film at a rate of  $64\,\mu L\,cm^{-2}$  and spin-coated at 6000 rpm using a spin coater (WS-400-6NPP-LITE, Laurell). Post-application of the diluted acrylic resin on the AZO thin film, the film underwent a natural drying process under varying conditions for 5 min. These drying conditions ranged from 18 to 28 °C in temperature and from 10% to 40% relative humidity (RH). To maintain consistent temperature and humidity levels, the spin-coating and drying steps, crucial for inducing cracks on the acrylic film, were conducted inside a glove box.

The drying conditions led to the formation of various structures on the coated acrylic resin films, characterized by differing widths and quantities of cracks. These cracked acrylic films, henceforth referred to as cracked templates,

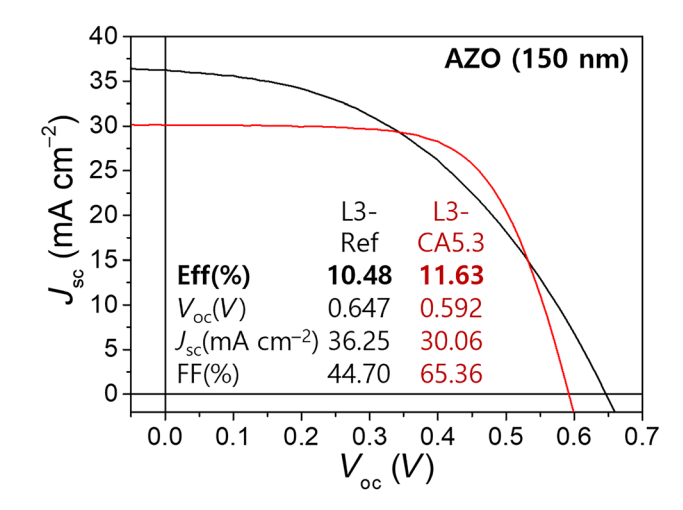


**Figure 5.** The current-voltage (J-V) curves for L3-Ref and L3-CA5.3 samples. The CIGS solar cells in the L3 series feature a 150 nm AZO thin film, in contrast to the 350 nm used previously.

were employed in the fabrication of a metallic network electrode. A thin film of Ag,  $\sim\!200\,\mathrm{nm}$  thick, was deposited onto the cracked template via RF sputtering at a power of 30 W for a duration of 30 min. During the Ag thin film deposition within the cracks, the film's thickness diminished to  $\sim\!150\,\mathrm{nm}$ , consequently reducing the actual thickness of the Ag networks. Following this, the cracked template with the Ag thin film was separated from the AZO thin film through ultrasonic cleaning for 5 min in isopropyl alcohol and deionized water sequentially. This process resulted in the retention of an Ag mesh-like network electrode on the AZO thin-film, forming a hybrid TCE, referred to as the hybrid TCE in this study.

Characterization of Ag network with AZO thin film: For the structural characterization of the Ag network, surface images were captured using scanning electron microscopy (SEM; MIRA4, Tescan), as illustrated in Figure S6, Supporting Information. The widths, densities, and coverage areas of the Ag networks were quantified based on these images. In this analysis, the density of the Ag network is defined as the number of network lines per millimeter (mm), where a single network line is measured from one intersection point to the next, as depicted in Figure S6, Supporting Information. The width, density, and CA of the Ag networks were calculated using MATLAB, with a detailed description of the programming process available in a previous study. [27] Given that a single SEM image does not adequately represent the Ag network structure of one sample, 16 SEM images were captured for each sample, and the average values of the three parameters were computed.

The optical and electrical properties of the hybrid TCEs were evaluated through measurements of transmittance and  $R_{\rm sh}$ , using a spectrophotometer (Spectro 22RS, LAbomed) and a four-point-probe resistivity meter (RC2175, EDTM), respectively. Each measurement was repeated at least thrice per sample, with the average values being utilized in this study. The FOM for the TCE was calculated from the average values of transmittance and  $R_{\rm sh}$  using Equation (1): $1^{1.4,17}$ 

$$FOM = \frac{188.5}{R_{sh} \left( T^{-\frac{1}{2}} - 1 \right)},\tag{1}$$

where  $R_{\rm sh}$  represents the sheet resistance and T represents the transmittance at a wavelength of 550 nm.

Fabrication and characterization of CIGS solar cells: For the CIGS layer, an absorber film with a thickness of 2.3  $\mu m$  was deposited on soda lime glass coated with Mo utilizing a three-step co-evaporation process. Prior to the deposition of the absorber, an ultrathin layer of Ag  $\sim\!10$  nm thick was deposited onto the Mo back contact using DC sputtering. In the initial stage of the co-evaporation process, In, Ga, and Se were evaporated onto the Mo layer at a relatively low temperature of around 340 °C. To optimize the gallium grading in the bandgap (GGI),

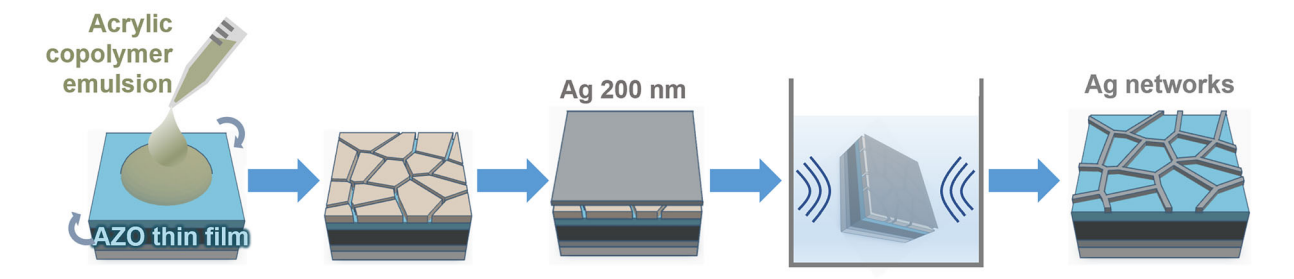


Figure 6. The process of Ag network formation on an AZO thin film.

the Ga shutter was opened for 10 min in a selenium-rich environment before commencing this stage. In the subsequent stage, Cu and Se were evaporated at a higher substrate temperature of  $\sim \! 580\,^{\circ}\text{C}$  until the formation of a Cu-rich CIGS phase. Finally, additional In and Ga, along with Se, were evaporated onto the substrate, maintaining the same temperature as in the second stage, to achieve a Cu-poor CIGS phase. Following the formation of the CIGS layer, the cells were coated with a cadmium sulfide (CdS) buffer layer, 50 nm thick, using chemical bath deposition. The front contact layers comprised an intrinsic zinc oxide (i-ZnO) layer  $\sim \! 50$  nm thick and an AZO window layer about 350 nm thick, both applied using RF sputtering.

For the metallic electrode implementation on the AZO thin film of a CIGS solar cell, two types were prepared: a Ag mesh-like network and an Al metallic grid. The Ag network electrode for the set1 series was fabricated utilizing the methodology outlined in section 2.1. To vary the coverage areas of the Ag network, the Ag networks for the set2 and set3 samples were produced by adjusting the spin-coating speed from 2000 to 8000 rpm, while the temperature and humidity conditions during the drying process were kept constant. An Al metallic grid, serving as a reference for the CIGS solar cell, was deposited on the AZO layer of the CIGS solar cell for charge collection. This grid, covering an area of 0.2025 cm<sup>2</sup>, was created through thermal evaporation using a mechanically defined shadow mask. Images depicting the Al grids and Ag networks on the small-area CIGS solar cells (0.2025 cm<sup>2</sup>) are presented in Figure S7, Supporting Information. For large-area CIGS solar cells (1.0609 cm<sup>2</sup>), such as those in the L1, L2, and L3 set samples, no metallic grid was applied on the TCO, unlike in the solar module configuration. These large-area cells were prepared both with and without an Al grid for reference, as well as with the Ag network, to facilitate a comparative analysis of their properties.

The fabrication of the CIGS solar cells, from the CIGS absorber layer to the AZO thin film, for each set of samples, including the reference cell, was conducted simultaneously. This concurrent fabrication approach was adopted to enable a comprehensive comparison of the solar cell properties depending on the type of electrode used. In the L3 set of samples, the AZO layer's thickness was reduced from 350 to 150 nm. This modification aimed to assess the effectiveness of the Ag network in a CIGS solar cell featuring a thinner AZO film.

The power conversion efficiency (Eff) of the CIGS solar cell was determined using a solar simulator (94022A, Newport Co.) under AM 1.5 illumination at a power density of 100 mW cm $^{-2}$  (1 sun). Additional performance metrics such as current–voltage (J-V) curves, open-circuit voltage ( $V_{\rm oc}$ ), short-circuit current ( $I_{\rm sc}$ ), and fill factor (FF) were also acquired. The EQE of the cells was measured using EQE equipment (McScience) equipped with a Xe lamp source. In this study, two cell sizes were examined: a small area of 0.2025 cm $^2$  and a large area of 1.0609 cm $^2$  for the CIGS solar cells. It is important to note that these areas include the metallic grid and/or the Ag network, distinguishing them from the active area. All conversion efficiencies were ascertained without the application of an antireflection coating or a PDT process. The SEM images and structural properties of the Ag networks on the CIGS solar cells were obtained as previously described.

#### **Acknowledgements**

H.Y., H.V.Q. and I.L. contributed equally to this work. The research presented in this article received substantial support from a series of grants provided by the

National Research Foundation of Korea (NRF). The specific grants that facilitated this study include No. 2021R1A5A8033165, RS-2023-00249229, 2022M3J1A 1085371, and 2023R1A2C1007386. Additionally, this work was supported by the Human Resource Program in Energy Technology of the Korea Institute of Energy Technology Evaluation and Planning (KETEP), under grant No. 20214000000200. These grants were funded by the Ministry of Science and ICT (MSIT), the Ministry of Education, and the Ministry of Trade, Industry & Energy of the Republic of Korea

#### **Conflict of Interest**

The authors declare no conflict of interest.

#### **Supporting Information**

Supporting Information is available from the Wiley Online Library or from the author

#### **Keywords**

CIGS, large-area solar cell, metal mesh, metallic network, transparent electrode

Received: January 30, 2024 Revised: March 19, 2024 Published online: April 8, 2024

- [1] V. Bermudez, A. Perez-Rodriguez, Nat. Energy 2018, 3, 466.
- [2] A. Anand, M. M. Islam, R. Meitzner, U. S. Schubert, H. Hoppe, Adv. Energy Mater. 2021, 11, 2100875.
- [3] J. M. C. da Silva Filho, A. D. Goncalves, F. C. Marques, J. N. de Freitas, Sol. RRL 2022, 6, 2100865.
- [4] K. Gensowski, T. Freund, S. Tepner, F. Clement, Phys. Status Solidi Rapid Res. Lett. 2022, 16, 2200040.
- [5] J. van Deelen, C. Frijters, Sol. Energy 2017, 143, 93.
- [6] J. van Deelen, M. Barink, L. Klerk, P. Voorthuijzen, A. Hovestad, Prog. Photovolt. Res. Appl. 2015, 23, 498.
- [7] J. van Deelen, L. Klerk, M. Barink, Sol. Energy 2014, 107, 135.
- [8] D. S. Hecht, L. Hu, G. Irvin, Adv. Mater. 2011, 23, 1482.
- [9] B. Han, Q. Peng, R. Li, Q. Rong, Y. Ding, E. M. Akinoglu, X. Wu, X. Wang, X. Lu, Q. Wang, G. Zhou, J.-M. Liu, Z. Ren, M. Giersig, A. Herczynski, K. Kempa, J. Gao, Nat. Commun. 2016, 7, 12825.
- [10] S. Kiruthika, R. Gupta, K. D. M. Rao, S. Chakraborty, N. Padmavathy, G. U. Kulkarni, J. Mater. Chem. C 2014, 2, 2089.
- [11] K. J. Prince, C. P. Muzzillo, M. Mirzokarimov, C. A. Wolden, L. M. Wheeler, ACS Appl. Energy Mater. 2022, 5, 9273.

- [12] K. S. Cho, S. Kang, Y.-J. Oh, J. S. Park, S. Lee, J.-S. Wi, J.-H. Park, S. Song, K. Kim, Y.-J. Eo, J. H. Yun, J. Gwak, J.-S. Cho, C.-H. Chung, ACS Appl. Electron. Mater. 2022, 4, 823.
- [13] A. Kurmar, G. U. Kulkarni, J. Appl. Phys. 2016, 119, 015102.
- [14] J. Gao, Z. Xian, G. Zhou, J.-M. Liu, K. Kempa, Adv. Funct. Mater. 2018, 28, 1705023.
- [15] Y. Han, Z. Hu, W. Zha, X. Chen, L. Yin, J. Guo, Z. Li, Q. Luo, W. Su, C.-Q. Ma, Adv. Mater. 2022, 34, 2110276.
- [16] Q. Peng, S. Li, B. Han, Q. Rong, X. Lu, Q. Wang, M. Zeng, G. Zhou, J.-M. Liu, K. Kempa, J. Gao, Adv. Mater. Technol. 2016, 1, 1600095.
- [17] B. Han, K. Pei, Y. Huang, X. Zhang, Q. Rong, Q. Lin, Y. Guo, T. Sun, C. Guo, D. Carnahan, M. Giersig, Y. Wang, J. Gao, Z. Ren, K. Kempa, Adv. Mater. 2014, 26, 873.
- [18] R. Gupta, K. D. M. Rao, S. Kiruthika, G. U. Kulkarni, ACS Appl. Mater. Interfaces 2016, 8, 12559.

- [19] C. P. Muzzillo, M. O. Reese, L. M. Mansfield, ACS Appl. Mater. Interfaces 2020, 12, 25895.
- [20] X. Chen, W. Guo, L. Xie, C. Wei, J. Zhuang, W. Su, Z. Cui, ACS Appl. Mater. Interfaces 2017, 9, 37048.
- [21] Z. Wang, B. Jiao, L. Huang, X. Zuo, W. Zhang, Y. Li, J. Wang, H. Dong, X. Hou, Z. Wu, ACS Appl. Mater. Interfaces 2021, 13, 41836.
- [22] V. Raman, Y.-H. Cho, H.-M. Kim, Y.-J. Kim, H.-M. Sim, H.-K. Kim, Ceram. Int. 2021, 47, 27230.
- [23] Y.-G. Kim, Y. J. Tak, H. J. Kim, W.-G. Kim, H. Yoo, H. J. Kim, Sci. Rep. 2018, 8, 5546.
- [24] Z. Zeng, C. Wang, J. Gau, J. Appl. Phys. 2020, 127, 065104.
- [25] Y. Yang, F. Min, Y. Qiao, Z. Li, F. Vogelbacher, Z. Liu, W. Lv, Y. Wang, Y. Song, Nano Energy 2021, 89, 106384.
- [26] C. P. Muzzillo, Adv. Energy Mater. 2022, 12, 2103119.
- [27] S. T. Jo, Master's Thesis, Kyungpook National University Graduate School, 2024.